ACS APPLIED MATERIALS & INTERFACES

Research Article

www.acsami.org

Engineering Preferential Adsorption of Single-Walled Carbon Nanotubes on Functionalized ST-cut Surfaces of Quartz

Juan C. Burgos[‡] and Perla B. Balbuena*[,†,‡]

[†]Department of Chemical Engineering and [‡]Department of Materials Science and Engineering, Texas A&M University, College Station, Texas 77843, United States

Supporting Information

ABSTRACT: Horizontal alignment during synthesis of single-walled carbon nanotubes has been found experimentally along certain directions of well-defined quartz surfaces. The reasons for such alignment are here examined using first-principles computational analysis, as a function of structure and chemistry of the specific exposed facet, presence and location of OH and H functional groups, and degree of hydration of the surface. It is found that selective functionalization of low-coordinated surface sites may cause exposure of low-coordinated Si atoms that bond strongly to nanotube walls. On the other hand, saturation of low-coordinated oxygen also favors carbon nanotube adhesion to the substrate. As found previously on bare silica surfaces, a chirality preference is confirmed on functionalized surfaces toward zigzag over armchair nanotubes. Magnetization effects on the surface originated by the presence of adsorbed functional groups are found to enhance adsorption of arm-chair nanotubes compared to that on clean surfaces. On the basis of the findings, it is suggested that surfaces may be engineered to favor horizontal adsorption of specific chiralities along preferential directions.

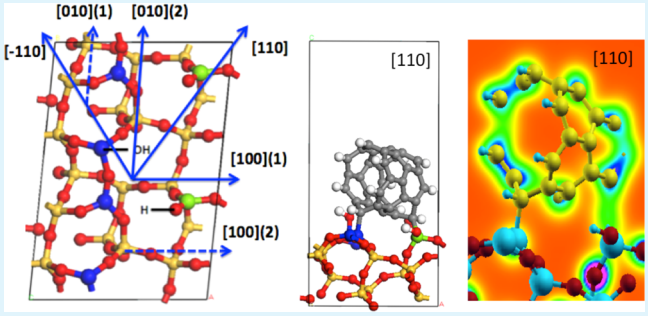

KEYWORDS: *density functional theory, single-walled carbon nanotubes, adhesion nanotube/substrate, horizontal growth, hydroxylated quartz surfaces, chirality preference*

INTRODUCTION

Carbon nanotubes arose into the scientific spotlight in 1991,[1] and since then they have been the focus of numerous studies aiming to characterize them mechanically and electronically. These novel materials have shown excellent mechanical, electronic, and optical properties that led them to meet performance standards required for various technological applications.[2−4] Among their potential high technology applications, field effect transistors are devices in which single-walled carbon nanotubes (SWCNTs) may satisfy performance demands because of their outstanding thermal conductivity, mobility, and mechanical stability.[5−7] Nevertheless, two main drawbacks prevent carbon nanotubes achieving high performance in field effect transistors: the lack of chirality selectivity and alignment on dielectric substrates during growth. Chirality is the structural variable that defines carbon nanotubes electronic band structure, and it is perhaps the most difficult property to be controlled during chemical vapor deposition (CVD) synthesis, in spite of significant advances in this field.[8−10] While researchers continue investing significant efforts on finding reliable methods to produce bundles with homogeneous chiralities, the alignment of SWCNTs in the bundle remains an issue obstructing the development of fully functional SWCNT-based electronic devices.

Experimental strategies have been proposed to guide nanotubes along specific directions on insulator substrates such as silicon oxide. Liu and co-workers[11] achieved growing of horizontally aligned SWCNTs on the stable temperature cut (ST-cut) surface of quartz, whose crystallographic plane was identified as the (01 $\bar{1}$ 1) by X-ray diffraction techniques.[12] The approach consisted on patterning the quartz surface by drawing parallel lines of catalyst nanoparticles from which carbon nanotubes grow.[11] Through this method, SWCNT root growth was favored over tip growth, whereas surface diffusion and collision of catalyst particles were suppressed. The absence of catalyst sintering and Ostwald ripening led to high density of horizontally aligned carbon nanotubes with narrow diameter distributions. Liu and co-workers[11] attributed nanotube bending during growth to an increase in catalyst and nanotube diameters and the consequent loss in preferential epitaxial interactions along the *x*-axis of the ST-cut surface, which has monoclinic unit cell (Figure 1). Conversely, other authors have concluded that the bending angle, which may be observed in the growth direction, is directly related to the angle of the O−Si−O segments of the quartz surface.[12] Liu et al. later determined that the direction of alignment was exclusively

Received: April 30, 2014
Accepted: July 15, 2014
Published: July 15, 2014

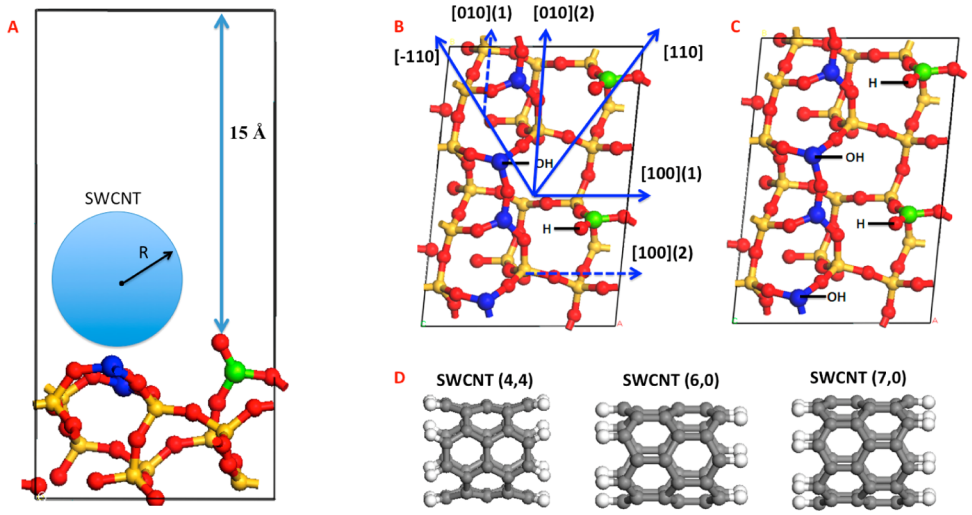

Figure 1. ST-cut surface of quartz, which corresponds to the (01 $\bar{1}$ 1) plane of the hexagonal lattice. (A) Side view. Blue atoms, unsaturated Si atoms; yellow, saturated Si; red, O atom; and green, unsaturated Si bonded to unsaturated O. The distance between the unsaturated oxygen and the top of the cell gives the vacuum, calculated as 15 Å. Nanotubes with diameter 2*R* are fit within the cell. The diameters are 5.43, 4.70, and 5.48 Å, for SWCNTs (4,4), (6,0), and (7,0), respectively. (B) Top view for the monohydrated surface. Four directions indicated by solid blue arrows. The dashed blue arrow indicates parallel positions along *x*: [100](2) and *y*: [010](1) axes. (C) Top view for dihydrated surface. (D) Three finite length nanotubes placed on the surfaces.

governed by epitaxial interactions between the outer shell of carbon nanotubes and the catalyst support surface,[13] although surface annealing may be critical on enhancing horizontal alignment of carbon nanotubes.[12] Moreover, our recent density functional theory (DFT) calculations demonstrated that patterns delineated by silicon and oxygen atoms along the [010] direction establish the strongest adsorption energy for zigzag nanotubes, and the weakest for armchair nanotubes.[14] This suggests that the nanotube electronic band structure is a key factor on the preferential adsorption of carbon nanotubes. We thus demonstrated that patterns delimited by silicon and oxygen atoms guide growing nanotubes along preferential directions via specific electronic interactions. However, our earlier study neglected the presence of different species in the feedstock gas phase that may functionalize unsaturated silicon and oxygen atoms on the surface topmost layer, therefore altering preferential growth directions.

Water, methanol, ethanol, and other alcohols are some of the precursor and inert compounds fed into CVD reactors to grow carbon nanotubes. These species tend to release OH radicals and hydrogen into the system. The effect of OH radicals from alcohol and water dissociation has been extensively reported as a factor enhancing the semiconducting selectivity and SWCNTs density.[8,15] The nanotube selectivity has been commonly attributed to selective etching of metallic tubes based on observations of reduced density of SWCNTs grown on ST-cut quartz and the lower ionization potential of the metallic nanotubes that makes them vulnerable in oxidative environments.[8,15] Nonetheless, alignment has not been associated with the presence of OH radicals on the system, although it is known that products of water dissociation can hydrate, hydrogenate or hydroxylate surfaces modifying their reactivity toward adsorbates.[16] Even in the case of no dissociation, water molecules can alter the adsorption behavior of adsorbates on a surface.[17] In this study, we present a detailed DFT analysis of the effect of quartz surface functionalization on the horizontal alignment and chiral preferences on nanotube adsorption. New insights allow us to suggest directions toward engineering quartz surfaces to achieve preferential alignment of specific chiralities.

COMPUTATIONAL METHODS

DFT calculations were carried out using the Vienna ab initio simulation package (VASP).[18,19] The code describes electronic interactions by the projector-augmented (PAW)[20] method, which is expanded within plane wave basis sets. Only plane waves with kinetic energies below 400 eV were included in the basis set. The Perdew–Burke–Ernzerhoff (PBE) exchange model,[21] which is a generalized gradient approximation (GGA) function, was employed to describe the electron exchange and correlation effects. Because of the semiconducting and insulating character of the system, the partial occupancies were set to each orbital following the tetrahedron method with Blochl corrections.[22] The smearing width was established in 0.1 eV. Convergence criteria were set to 1×10^{-4} and 1×10^{-3} for electronic and ionic minimizations, respectively, whereas a $5 \times 5 \times 1$ Monkhorst pack grid[21] was used for the Brillouin zone integrations carried out over the system. For the DOS calculations, a single ionic step was performed increasing the Monkhorst pack grid for Brillouin zone integration to $10 \times 10 \times 1$, and increasing the number of grid points in the density of states to 2000.

After an exhaustive literature review, we have established the thermodynamic phase and the crystallographic plane corresponding to the ST-cut surface of quartz at growth conditions. The ST-cut quartz was identified as the (01 $\bar{1}$ 1) crystallographic plane of the β-quartz, which lies at 42° from the *y*-axis approximately. Detailed information about the Miller indices selection can be found in our previous report.[14] This surface was chosen for our DFT calculations because of its remarkable selectivity and capability for induction of alignment, which have been observed experimentally when nanotubes grow horizontally on this type of substrate. We constructed our surface using the surface cleavage tool of the Materials Studio package.[23] The surface was modeled using a 1×2 supercell with 4 layers of thickness and 15 Å vacuum (Figure 1A). Each layer is composed by 6 Si atoms and 12 O atoms, which keep the stoichiometric relation of silica. Low saturated Si and O atoms in the topmost layer of the surface were targeted for saturation with hydroxyl radicals (*OH) and hydrogen atoms (H), respectively. Different combinations resulted in different OH terminations and concentrations on top layer of the surface (Figures 1B, 1C, 7C (inset), and 8B). Three different SWCNTs were optimized and placed on top of the surface along different directions.

SWCNTs (4,4), (6,0), and (7,0) with finite lengths were fit in the unit cell and saturated with hydrogen atoms at the open edges (Figure 1D) to minimize the effect of the dangling bonds. The molecular formulas for SWCNTs (4,4), (6,0), and (7,0) correspond to $C_{40}H_{16}$, $C_{36}H_{12}$, and $C_{42}H_{14}$, respectively. Electronic band structure calculations of SWCNTs have shown that all armchair nanotubes are metallic, whereas zigzag nanotubes are semiconductors with a band gap width dependent upon their chiral indices (n,m).[24,25] With the selection of our three nanotubes, we are considering three possible electronic behaviors. SWCNT (4,4) is metallic ($n - m = 0$). Chiral indices (7,0) correspond to a semiconducting tube with a moderate band gap ($n - m \neq 3k$, $k = 1, 2, 3, \ldots$). The remaining zigzag tube (6,0) is a narrow-gap semiconductor ($n - m = 3k$, $k = 1, 2, 3, \ldots$), although it has been found to be metallic because of hybridization of σ^* and π^* orbitals that results from the tube small diameter.[26] In total, 6 positions corresponding to 4 crystallographic directions were tested for each nanotube (Figure 1B). Eighteen calculations (3 nanotubes on 6 positions) were made for each one of the four surface terminations.

RESULTS AND DISCUSSION

Water Dissociation on Silica Surfaces. Water is one of the nonreactive species added in a CVD process together with inert gases such as argon or helium. At SWCNT synthesis conditions (~1000 K and moderate pressures close to 1 atm), high kinetic energy water molecules are found in vapor phase. As a part of the gas phase mixture, although it does not participate on the reaction directly, water can interact with carbon precursor molecules, catalyzed carbon from the nanotube, metal atoms from the catalyst, or atoms on the surface of the catalyst support. Both metallic surfaces and silicon oxide surfaces have been shown to catalyze the dissociation of water molecules into hydroxonium and hydroxyl ions.[27−33] Reaction pathways and energy landscapes have been detailed.[34] ab initio molecular dynamics (AIMD) simulations of a water molecule over quartz (100), (110), and ST-cut surfaces were carried out at 1000 K. AIMD simulations were performed following the Born−Oppenheimer procedure to describe the classical motion of ions, as implemented in VASP. As in the case of relaxation of SWCNTs on quartz, the GGA-PBE functional was used with a plane wave energy cutoff of 400 eV. The time step was set to 1 fs, and the systems were allowed to run enough time until water molecules dissociated or moved away from the substrate; this step corresponded to ~300 fs. The canonical ensemble with the Nosé algorithm to control the frequency of temperature oscillations was used. The Nosé-mass parameter was set to 0.5. Because of the high temperature and associated high kinetic energy and the very low water density, the water molecule rarely interacts with the studied surfaces, except for the case of quartz (110), where a water molecule dissociates on the substrate topmost layer due to the presence of low coordinated surface atoms (Figure 2). The AIMD simulations reveal a mechanism by which water molecules are dissociated on a silica surface. SiO_2 (quartz) (110) surfaces have both unsaturated O and Si atoms. The Si−O bond has a covalent component that has been estimated in 50%, although the ionic character increases in detriment of the covalent component when the coordination of atoms decreases.[35] Hence, the water molecule dissociates on the quartz (110) surface as a consequence of a proton transfer from water to a negatively charged low coordinated O atom of the top layer. Once the proton is attached to this oxygen, no further surface atomic diffusion was evidenced. Meanwhile, the released OH ions diffuse through the surface until they attach strongly to low

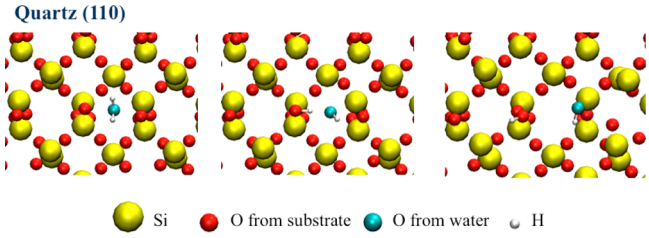

Figure 2. Water dissociation mechanism on quartz (110). Hydronium ion transfers to low coordinated O at the top of the surface. Hydroxyl ion migrates until finding an unsaturated Si atom and forming a Si−OH bond.

coordinated Si atoms at the topmost layer, creating Si−OH surface terminations.

On the basis of the AIMD results, DFT simulations were carried out on ST-quartz surfaces functionalized with water dissociation products. We assume that this dissociation should also occur on the ST-cut surface of quartz since all silica surfaces studied share similar terminations with unsaturated Si and O atoms. Based on the concentration of unsaturated oxygen atoms in the surface unit cell, two water molecules represent the maximum capacity of the surface to chemisorb water through dissociation, proton transfer, and saturation of low coordinated atoms. Therefore, one and two molecule(s) represent water concentrations of 50 and 100%, respectively. dihydrated surfaces is then the maximum concentration of water products per surface area.

A total of six surface low-coordinated Si atoms were identified, four at the top layer and (blue atoms in Figure 1) two at the subsurface (green atoms in Figure 1). Two low-coordinated surface O atoms are bonded to low-coordinated Si in the subsurface, as shown in Figure 1A. Thus, functional groups can saturate these atoms and define surface terminations with different OH concentrations and locations.

Adsorption of SWCNTs on the Hydrated Surfaces. SWCNTs (4,4), (6,0), and (7,0) (Figure 1D) were deposited along six different directions of the monohydrated (one water molecule per unit cell) and dihydrated (two water molecules per unit cell) surfaces (Figure 1) separated from the top periodic image by a vacuum space of 15 Å (Figure 1A). Figure 3A shows for a monohydrated surface similar trends to the ones reported previously for clean surfaces.[14] The (4,4) armchair tube is not energetically favored for alignment along any

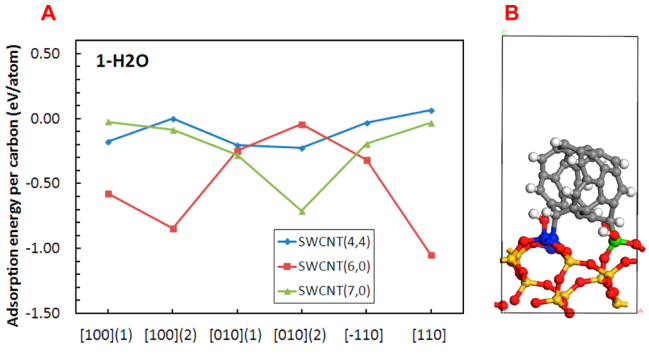

Figure 3. (A) Adsorption energy per carbon atom in contact with surface for three different nanotubes on the monohydrated surface (top view in Figure 1B). The values are calculated along six surface directions. (B) Scheme representing the SWCNT (6,0) along the preferred [110] direction.

dx.doi.org/10.1021/am5026566 | ACS Appl. Mater. Interfaces 2014, 6, 12665−12673

direction. The metallic character of this tube and the significant differences in adsorption energy with respect to zigzag tubes, make evident the existence of an effect of the substrate on the preferential deposition of semiconducting tubes. In contrast, zigzag tubes were clearly favored to adsorb on the monohydrated surface of quartz, although SWCNTs (6,0) and (7,0) did not align preferentially along the same direction. For the case of the SWCNT (7,0), the direction parallel to the [010](2) *y*-axis was found to be the direction of strongest adsorption energy. Along this direction, nanotubes with a diameter within the range of the three nanotubes studied (∼5 Å) were exposed to close interactions with low-coordinated Si and O atoms. It is worth to note that this direction represented the strongest overall adsorption energy on the clean (non-hydrated) ST-cut surface of quartz.[14] In the hydrated surfaces, low saturated sites along that direction become saturated with products of water dissociation, i.e., having OH terminations side by side of the [010](2) direction (Figure 1B).

It is also remarkable that the nanotube (6,0) undergoes a very weak attraction along the same *y* direction. The nanotube (6,0) has a smaller diameter than the (7,0), which places it in disadvantage respect to the (7,0). This is because the [010](2) direction is characterized by having a channel delimited by low-coordinated Si atoms at the topmost layer and the subsurface. A nanotube with a larger diameter is able to reach the effect of low-coordinated Si atoms at both sides of the channel. On the other hand, semiconducting (7,0) and metallic (4,4) have very similar diameters but different adsorption strengths on this direction, which confirms that the electronic behavior of each nanotube defines its adsorption preferences.

Figure 3A also illustrates that (6,0) adsorbs preferentially along the [100](2) *x*-axis and on the [110] direction. Along these directions, the epitaxial interaction between the nanotubes (6,0) and the silica surface allows the nanotube (6,0) to maximize its contacts with unsaturated Si atoms at the subsurface (green atoms in Figure 3B), sometimes even repelling OH functional groups attached to them, as shown in Figure 3B. Thus, far, the results indicate that preferential adsorption is driven entirely by epitaxial interactions between C atoms and low-coordinated Si at the surface, suggesting that OH and O terminations play a minimal role. The effect of higher surface concentration of OH functional groups was analyzed on dihydrated surfaces (two water molecules per unit cell), as shown in Figure 1C. The results in Figure 4 indicate a similar adsorption pattern to that in Figure 3.

The only significant difference lies in the adsorption energies when the nanotube (6,0) is deposited on the [100](2) direction. This result is expected because the [100](2) direction is the only one where the concentration of OH terminations can be changed along the path where the tubes adsorb. Thus, the adsorption energy of the SWCNT (6,0) on the [100](2) direction is shifted from a moderately strong adsorption in the monohydrated surface to a null, almost repulsive interaction when additional OH functional groups saturate these surface sites in the dihydrated case. The reasons for this difference could be purely steric, or otherwise electronic. The steric argument would be valid if the OH group obstructs C atoms to access low-coordinated Si atoms at the subsurface. However, it has been observed that OH groups tend to be flexible when bonded to unsaturated Si (green atoms in Figure 1C), which allows deflection of the OH group and grants access of C atoms to interactions with unsaturated Si atoms. In contrast, the extra OH group in the nanotube path

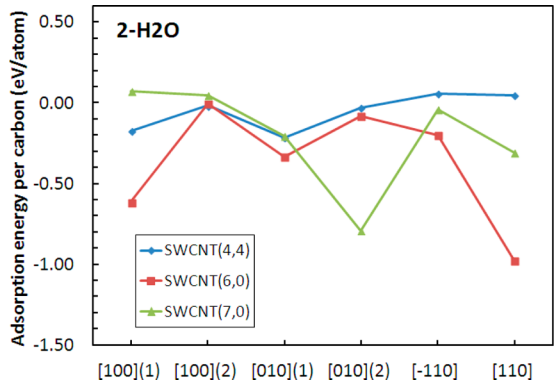

Figure 4. Adsorption energy per carbon atom in contact with the surface for three different nanotubes on the dihydrated surface. The values are calculated along six surface directions.

([100](2) direction) saturates a Si atom at the surface (blue atoms in Figure 1C), stabilizing the Si via formation of a stiff (nonflexible) Si−OH bond. Consequently, the steric explanation can be disregarded, and the change in the chemical character of a Si atom at the topmost layer of the surface remains as the only factor disrupting the adsorption trends from monohydrated to dihydrated surfaces. This result is strong evidence indicating the importance of Si atoms on defining preferential directions of alignment of nanotubes on a silica substrate. Therefore, the effect of OH radicals on the adsorption on quartz surfaces relies on modifications to the chemistry of Si surface atoms rather than on physical constraints because of changes on the surface topology. It is important to remark that a moderate hydration (defined here as monohydrated surface) of the ST-cut surface increases significantly the preferential alignment of nanotubes toward directions parallel to the *x*-axis, respect to the clean surface, as seen by comparing Figure 3A with Figure S4 in the Supporting Information. SWCNT (7,0), however, remains favoring the *y*-axis for adsorption no matter the degree of hydration.

We note that the results in Figures 3 and 4 do not include surface dipole corrections. To verify the effect of this correction on the adsorption energies, we repeated the calculations and the results are reported in Figures S5 and S6 in the Supporting Information. The results indicate that there is a small change in the adsorption energies that become ∼0.1 eV weaker when surface dipole corrections are included, however the trend discussed in Figures 3 and 4 is kept.

To confirm our hypothesis of Si atoms governing the alignment of carbon nanotubes along specific directions, we performed a charge density mapping for selected cases. From previous work[14] it is known that the strongest adsorption energies are characterized by a high population of charges at the interface between nanotubes and the silica support. For the monohydrated surface along the [100](2) direction, only the SWCNT (6,0) exhibits significant concentration of charges, up to 0.7 e/Å^3 at the interface between carbon and silicon atoms. SWCNTs (4,4) and (7,0) do not exchange charges at the interface, not even over unsaturated Si atoms, which suggests a correlation between the nanotube electronic properties and their ability to carry charges toward the interface (Figure 5A). Moreover, the strongest adsorption energy on the monohydrated surface was observed for the SWCNT (6,0) along the [110] direction. This direction has the uniqueness of facilitating formation of two C−Si bonds along the nanotube path (Figure

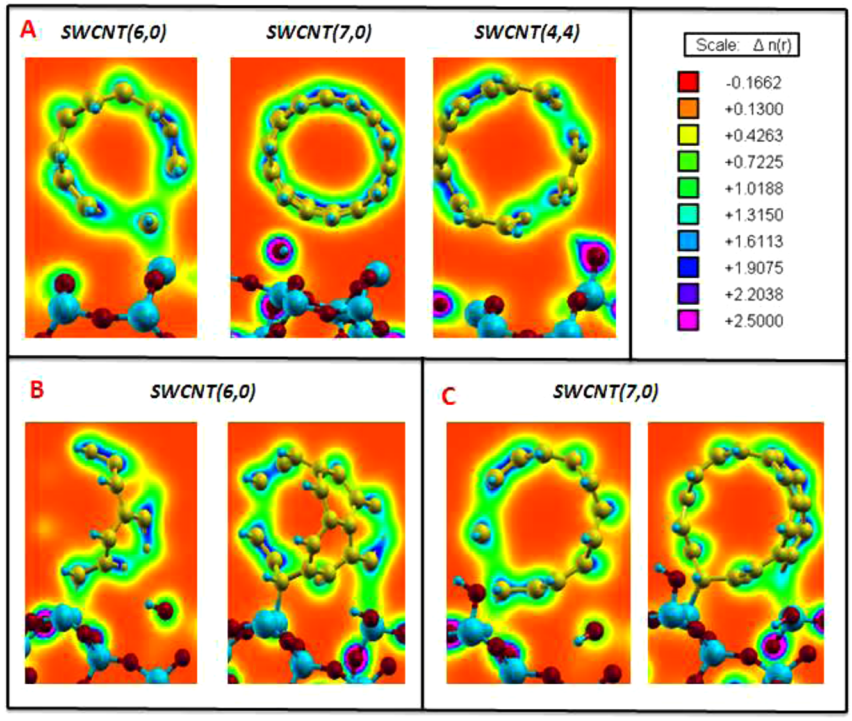

Figure 5. Charge density mapping for (A) SWCNT (6,0), (7,0), and (4,4) along [100](2) of the monohydrated surface, (B) SWCNT (6,0) along [110] of the monohydrated surface, (C) SWCNT(7,0) along the *y*-axis [010](2) of the dihydrated surface. The color chart displays ranges of charge densities in e/Å^3.

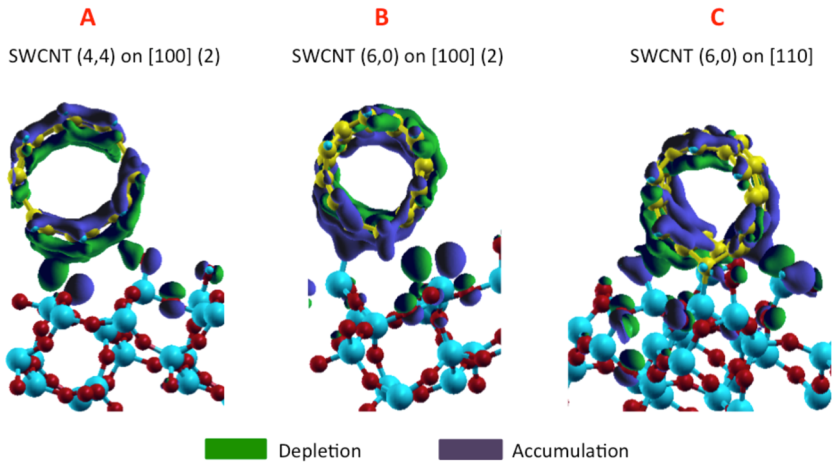

Figure 6. Charge density difference analysis for three different cases. (A, B) Cases on the monohydrated surfaces. (C) Case on the dihydrated surface.

3B), which allows concentrating charges at the interface in the order of 0.8−1.0 e/Å^3. Figure 5B shows the repulsion that causes the deflection of the OH functional group bonded to the unsaturated Si. The flexibility of this Si−OH bond allows a direct charge transfer at the interface between unsaturated Si and C atoms, as seen in Figure 5B. On the dihydrated surface, charge density maps along the *y-axis* shows how the SWCNT (7,0) reaches Si atoms on both sides of its path thus maximizing charge sharing at the interface (Figure 5C).

DFT analysis shows that nanotubes strongly adsorbing on the ST-cut surface of quartz experience structural deformations that led C atoms to reach points of interaction with near-surface low-coordinated Si atoms. Furthermore, adsorption along preferential directions sometimes demands certain amount of surface reconstruction. OH functional groups deflection along the path of the nanotube may induce low-coordinated Si atoms located at lower surface planes to diffuse toward higher locations on the surface and interact with C atoms from the nanotube, as shown in the Supporting Information (Figure S1).

Along a given direction, nanotubes with similar diameters adsorb with different strengths on clean and hydrated surfaces. A general scenario of depletion and accumulation of charges before and after nanotube adsorption provides insightful information about the repulsive/attractive nature of each interaction and the migration of charges upon adsorption. Charge depletion and accumulation were computed for an isosurface value of 0.8 e/Å^3 for nanotubes along the [100](2) direction of the monohydrated surface. These results confirm the repulsion experienced by the (4,4) tube as charges are

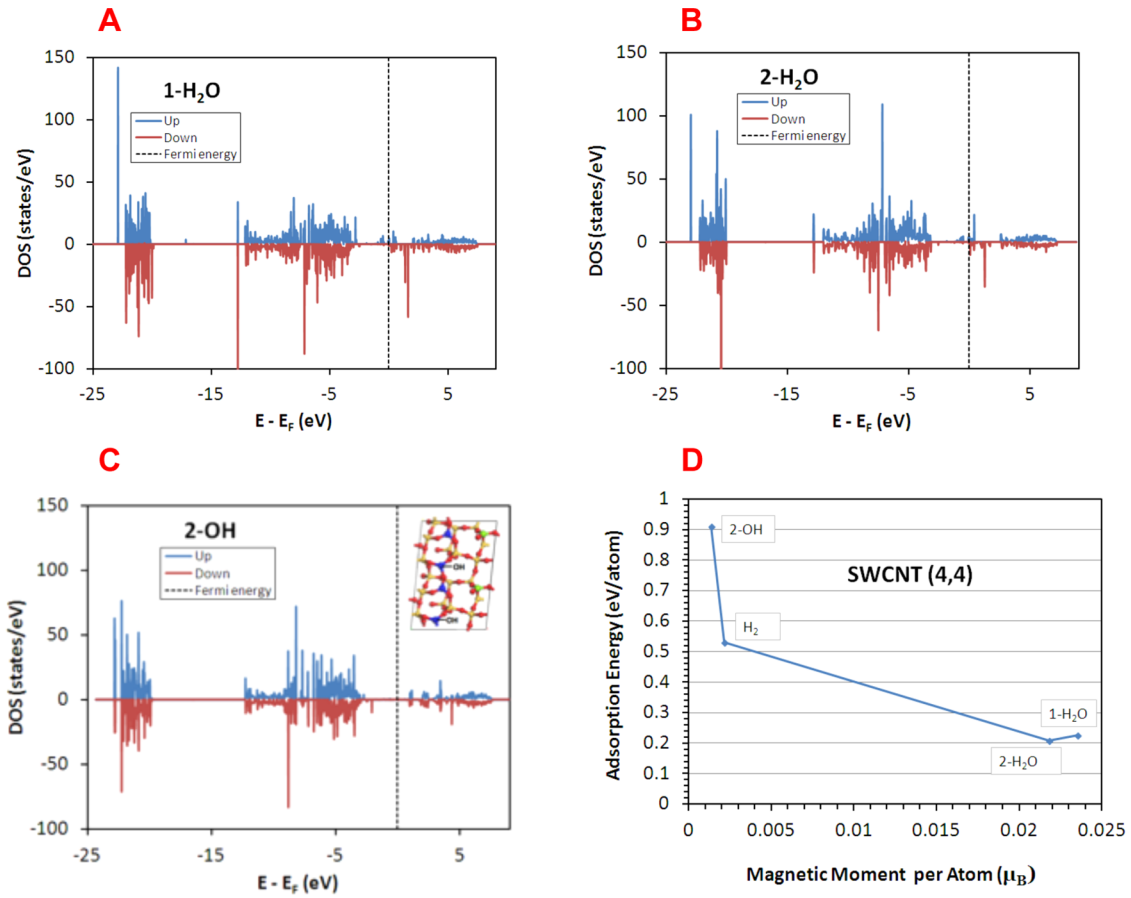

Figure 7. (A, B) Spin-resolved electronic DOS of atoms belonging to the two uppermost layers of hydrated surfaces. (C) Spin-resolved electronic DOS of atoms belonging to the two uppermost layers of hydroxylated surface. The inset represents the unit cell of the surface with its functionalization. (D) Adsorption energy per carbon atom as a function of surface magnetization and surface termination. The values reported correspond to the strongest adsorption found for SWCNT (4,4) on a given surface.

depleted at the interface and accumulated inside the nanotube, as seen in Figure 6A. In the top half of the (4,4) nanotube, charges are also displaced in the positive direction of the *z*-axis. This overall charge shift in the SWCNT (4,4) denotes a strong repulsion undergone by the nanotube after contact with the surface that results in a displacement of carbon nuclei away from the surface. In contrast, SWCNT (6,0) shows the strongest adsorption energy along the same direction of the monohydrated surface, and allows a significant charge accumulation at the interface. This is shown in Figure 6B, also illustrating electron depletion at the inner part for the lower nanotube half, as well as accumulation in the inner and depletion in the outer part of the upper half of the nanotube wall.

Electron cloud depletion at the interface was occasionally observed for hydrated surfaces, unlike the behavior on clean surfaces. Localized migration of charges away from the interface combined with accumulation at Si−C connections, are a result of structural deformation of strongly adsorbed nanotubes. As a consequence of these deformations, nuclei might move away from the surface at specific locations, such as stiff OH functional groups, and approach lower energy spots such as unsaturated Si sites. Therefore, simultaneous electron depletion and accumulation is observed at different points of the interface, as shown in Figure 6C for the (6,0) tube along the [110] direction of the dihydrated surface.

This analysis allows us to conclude that low-coordinated Si atoms guide preferential alignment of carbon nanotubes on the ST-surface of quartz. It was previously reported[14] that unsaturated O atoms at the surface were critical on defining preferential alignment through partial oxidation of nanotubes. However, here we demonstrate that if the low-coordinated O is bonded to low-coordinated Si, as in the case of the ST-cut, the unsaturated Si is most likely to cause the attraction and charge concentration at the interface. We believe these results can be extended to any kind of silica surface no matter the spatial arrangement of atoms within the lattice. Only the coordination states of the Si and O atoms will define the adsorption strength of carbon nanotubes on the surface, and therefore, the surface concentration and distribution of this kind of atoms will establish the directions of preferential alignment.

Adsorption and Surface Magnetization. Preferential adsorption of finite length zigzag SWCNTs on clean quartz surfaces was associated with asymmetric population of spin up and down states (spin polarization), not observed in finite length armchair nanotubes.[14] The asymmetry in the electronic spin states of zigzag tubes adsorbed on a clean surface, and their magnetic moments suggest a possible magnetic dipolar interaction between tubes and surfaces. Here the electronic density of states (DOS) was calculated before and after adsorption and analyzed only for carbon atoms (H atoms and atoms Si and O belonging to the substrate were not included). The Supporting Information shows the spin-resolved DOS for

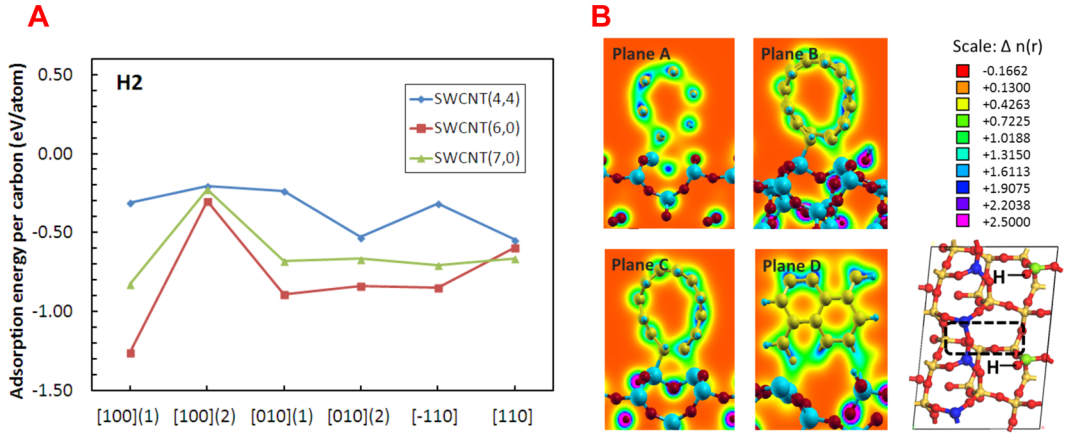

Figure 8. (A) Adsorption energy per carbon atom for three different nanotubes on the hydrogenated surface. The values are calculated along 6 surface directions. (B). Charge density mapping for SWCNT(6,0) along [100](1). Four different planes intersecting the main binding contacts are plotted. Plane D shows a lateral view that intersects two interacting spots that correspond to the same contacts of planes B and C. The dashed lines in the unit cell illustrate the approximate diameter of the (6,0) and how it interacts with three unsaturated Si atoms simultaneously. The color chart displays ranges for the charge density in e/Å^3.

the s and p-orbitals of each nanotube along the [110] (2) direction of monohydrated (see Figure S2 in the Supporting Information) and the [110] direction of the dihydrated (see Figure S3 in the Supporting Information) surfaces. DOS results are in agreement with previous results for finite length tubes on clean ST-cut surfaces.[14] Electronic states occupying narrow energy ranges that resemble van Hove singularities were observed. Furthermore, DOS plots showed break in the spin up/down symmetry of armchair tubes, depletion of the electronic states near the Fermi level as a result of strong interactions, and inner core states that become highly populated as a result of orbital hybridizations. Unlike preferential alignment trends, chiral preferences are not disturbed by surface functionalization with OH and hydrogen groups. However, these types of functionalizations introduce subtle modifications to the electronic DOS of surface atoms that might provide further clues on the alignment of SWCNTs. Thus, the spin-resolved DOS are plotted for atoms belonging to the two upper layers of each substrate, monohydrated and dihydrated surfaces. The DOS of hydrated surfaces are summarized in panels A and B in Figure 7, and can be compared with those for the clean surface.[14] The spin-resolved DOS plots for hydrated surfaces show higher population of electronic states at the Fermi level, compared to the clean surface. Furthermore, this relatively high density of electronic states at the Fermi level was accompanied by misbalance of spin up and spin down populations, which leads to spontaneous magnetization of the surface. The magnetic moments of the two top layers of these surfaces were computed as 0.024 and 0.022 μ_B per atom for mono and dihydrated surfaces, respectively. It was stated above that the magnetization of the surface may favor the adsorption of zigzag nanotubes through specific magnetic dipolar interactions. In contrast, this magnetization might be disfavoring an attractive interaction between armchair tubes and silica surfaces. Armchair tubes were not able to overcome the barrier of 0.25 eV/atom of adsorption energy along any direction of these magnetized hydrated surfaces. In order to confirm this hypothesis, a surface with a very symmetrical spin down/up DOS was found by saturating two Si atoms at the top of the surface (blue atoms) with two OH radicals (Figure 7C, inset). The surface configuration with two OH and two O terminations reduced the electronic population at the Fermi level to almost zero, as seen in Figure 7C. It also reduced the magnetic moment to 0.0014 μ_B per atom (Figure 7D). Interestingly, SWCNT (4,4) along the [100](2) direction of this surface adsorbed at 0.91 eV, which is the strongest adsorption observed for an armchair tube in our results.

Thus, proper functionalization may also induce preferential adsorption of specific chiralities due to electronic changes on the surface such as the suppression of surface magnetization.

Engineering Surface Functionalization. After having a better understanding of surface properties governing preferential alignment of horizontally deposited carbon nanotubes, a window opens to engineer surfaces seeking desired directions of alignment. According to the above discussion, a substrate that maximizes the density of low-coordinated Si atoms on the surface can be thought as enhancing the strength of adsorption of zigzag nanotubes. This can be achieved in the ST-surface of quartz by selectively saturating only the O terminations on the surface. There are two low-coordinated O atoms at the topmost layer, per unit cell of surface. Saturating these two atoms would represent a scenario in which the surface is hydrogenated. Note that during SWCNT growth, atomic hydrogen may be readily available through the catalysis of C-containing precursor gases at the high temperature CVD conditions. This surface will now have six unsaturated Si atoms on the surface, with two of them holding an OH functional group each, as seen in Figure 8B. This would eliminate the effect of unsaturated surface O that may cause partial oxidation of nanotubes, and would create flexible OH functional groups that are susceptible to deflection in the Si−OH bond orientation. After calculating the adsorption energies for finite length nanotubes on this surface, we found the strongest overall adsorption for SWCNT (6,0) along the *x*-axis, as seen in Figure 8A. This adsorption (1.26 eV/atom) is the strongest found in this and our previous work (see Figure S4 in the Supporting Information) The value overcomes the ∼1 eV/atom for SWCNT (6,0) on both hydrated surfaces along [110], and the 0.82 eV/atom for the SWCNT (7,0) along [010](2) of the clean surface (see Figure S4 in the Supporting Information). Despite the adsorption of SWCNTs (6,0) and (7,0) along the *y*-axis not being as strong as along the [100](1) direction, their adsorption values are close to the values reported for the clean surface, where the *y*-axis was the preferred direction of alignment. The SWCNT

(6,0) along [100](1) direction favors the direct interaction with three of the six low-coordinated Si surface atoms, as seen from the charge mapping analysis (Figure 8B). The interaction with one of them is achieved through repulsion of an OH functional group and consequent deflection of the Si−OH bond. Thus, the nanotube (6,0) aligns preferentially along the [100](1) direction through the creation of silicon "hangers" that keep the nanotube stuck to the silica support. The high density of low-coordinated Si along the perpendicular direction to the nanotube axis, allows the SWCNT (6,0) to stick to the substrate side by side and upfront, as seen in Figure 8B. It is worth noting that this direction was never found favorable for adsorption of any nanotube on any ST-cut surface in our previous studies. These findings are in agreement with the experimental results indicating the existence of preferential alignment parallel to the *x*-axis during horizontal growth.[8,12] In Liu's work,[8] methanol is added to the gas feedstock. OH radicals released from methanol were linked to the preferential etching of metallic caps and the consequent high population of semiconducting tubes. However, the OH radicals were never considered a factor for nanotube alignment along the *x*-axis. It should be pointed out that in the experiments performed by Liu and co-workers, a flow of molecular hydrogen is used during substrate treatment at 800 °C. On the other hand, Rutkowska et al.,[12] demonstrated alignment along the *x*-direction of the ST-cut surface of quartz. In their experiments, the furnace is preheated from room temperature to 700 °C in the presence of molecular hydrogen. H_2 is also part of the carbon feedstock along with CH_4.

The electronic DOS calculated for this surface evidenced reduced concentration of electronic states at the Fermi level and slight spin polarization, which gave a magnetic moment of 0.0021 μ_B per atom. Even though the SWCNT (6,0) was clearly favored for horizontal alignment on this surface, the hydrogenated surface allowed the SWCNT (4,4) to adsorb at 0.53 eV/atom along the [110] direction (Figure 8A). This value is stronger than the adsorption along any direction of hydrated surfaces, although it is weaker than the adsorption on the 2-OH surface. This is the inverse correlation followed by the magnetization of these surfaces, and supports our hypothesis of a trend showing decrease in armchair adsorption as the surface magnetic moment increases (Figure 7D).

We note that the nanotubes used in this report have short length. We are currently developing force fields for the interactions of carbon nanotubes with quartz surfaces which will be used in classical molecular dynamics simulations to test the effects of nanotube length and high temperatures on the nanotube/substrate adhesion properties. Preliminary results indicate good agreement between the DFT and MD results. Details will be published elsewhere.

CONCLUSIONS

DFT calculations yielded new insights into preferential adsorption of SWCNTs on quartz surfaces functionalized by water dissociation products. AIMD simulations demonstrated that water dissociation occurs on quartz surfaces producing hydrogen and OH radicals. OH radicals tend to bond low-coordinated Si atoms, whereas hydrogen saturates O atoms at the top of the surface, functionalizing the surface with OH terminations. It was demonstrated that horizontal alignment of SWCNTs on silica surfaces is governed by patterns drawn by unsaturated Si atoms at the topmost layer of silica surfaces. The saturation of O atoms with hydrogen to create OH terminations did not reduce the strength of adsorption of nanotubes. On the contrary, the strongest interactions between horizontal nanotubes and silica surfaces were observed along directions not containing unsaturated O. It was confirmed that for most of surface functionalizations the ST-cut surface of quartz favors the horizontal deposition of zigzag tubes over armchair ones. SWCNT (6,0) is preferred along the directions of strong adsorption, although the SWCNT (7,0) is energetically favored to align along the *y*-axis, following epitaxial ordering. SWCNT (4,4) adsorbs stronger on surfaces that present small to none spin polarization.

During the nucleation of carbon caps, carbon atoms dissolved inside the catalyst diffuse toward the catalyst surface, where they start nucleating carbon structures. Diffusion and precipitation of carbon atoms, cap nucleation, and the consequent nanotube alignment upon growth, might be influenced by the strength of interaction between carbon and the substrate. If the nucleated nanotube cap does not adsorb strongly to the support, we could observe vertical instead of horizontal growth. Here we show the preferential directions where horizontal growth may happen. After identifying the key elements defining preferential alignment, it is suggested that silica surfaces can be engineered to maximize the nanotube surface and guide nanotubes horizontally along specific directions.

ASSOCIATED CONTENT

Supporting Information

Figure S1 shows the surface reconstruction of the monohydrated surface as a result of a carbon nanotube horizontally deposited on it; Figure S2 illustrates electronic density of states for the all nanotubes before and after adsorption along the [110] direction of the hydrated surface;Figure S3 illustrates electronic density of states for the all nanotubes before and after adsorption along the [110] direction of the dihydrated surface; Figure S4 reports the adsorption energy per carbon atom for the (4,4), (6.0), and (7,0) nanotubes on clean ST-quartz surfaces; Figures S5 and S6 report the differences in adsorption energies when dipole corrections are included in the calculations for monohydrated and dihydrated surfaces, respectively. This material is available free of charge via the Internet at http://pubs.acs.org.

AUTHOR INFORMATION

Corresponding Author

*E-mail: balbuena@tamu.edu.

Notes

The authors declare no competing financial interest.

ACKNOWLEDGMENTS

This work was supported by the U.S. Department of Energy, Basic Energy Sciences, under Grant DE- FG02-06ER15836. Computational resources from TAMU Supercomputer Facility, Brazos Cluster at Texas A&M University, Texas Advanced Computing Center (TACC), and from the National Energy Research Scientific Computing Center, which is supported by the Office of Science of the U.S. Department of Energy under Contract DE-AC03-76SF00098, are gratefully acknowledged.

REFERENCES

(1) Iijima, S. Helical Microtubules of Graphitic Carbon. *Nature* **1991**, *354*, 56−56.

(2) Baughman, R. H.; Cui, C.; Zakhidov, A. A.; Iqbal, Z.; Barisci, J. N.; Spinks, G. M.; Wallace, G. G.; Mazzoldi, A.; De Rossi, D.; Rinzler, A. G.; Jaschinski, O.; Roth, S.; Kertesz, M. Carbon Nanotube Actuators. *Science* **1999**, *284*, 1340−1344.
(3) Ghosh, S.; Sood, A. K.; Kumar, N. Carbon Nanotube Flow Sensors. *Science* **2003**, *299*, 1042−1044.
(4) Tans, S. J.; Verschueren, A. R. M.; Dekker, C. Room-Temperature Transistor based on a Single Carbon Nanotube. *Nature* **1998**, *393*, 49−52.
(5) Bernholc, J.; Brenner, D.; Buongiorno Nardelli, M.; Meunier, V.; Roland, C. Mechanical and Electrical Properties of Nanotubes. *Annu. Rev. Mater. Res.* **2002**, *32*, 347−375.
(6) Pop, E.; Mann, D.; Wang, Q.; Goodson, K.; Dai, H. Thermal Conductance of an Individual Single-Wall Carbon Nanotube above Room Temperature. *Nano Lett.* **2005**, *6*, 96−100.
(7) Javey, A.; Kim, H.; Brink, M.; Wang, Q.; Ural, A.; Guo, J.; McIntyre, P.; McEuen, P.; Lundstrom, M.; Dai, H. High-[kappa] Dielectrics for Advanced Carbon-Nanotube Transistors and Logic Gates. *Nat. Mater.* **2002**, *1*, 241−246.
(8) Ding, L.; Tselev, A.; Wang, J.; Yuan, D.; Chu, H.; McNicholas, T. P.; Li, Y.; Liu, J. Selective Growth of Well-Aligned Semiconducting Single-Walled Carbon Nanotubes. *Nano Lett.* **2009**, *9*, 800−805.
(9) Harutyunyan, A. R.; Chen, G.; Paronyan, T. M.; Pigos, E. M.; Kuznetsov, O. A.; Hewaparakrama, K.; Kim, S. M.; Zakharov, D.; Stach, E. A.; Sumanasekera, G. U. Preferential Growth of Single-Walled Carbon Nanotubes with Metallic Conductivity. *Science* **2009**, *326*, 116−120.
(10) Chiang, W.-H.; Mohan Sankaran, R. Linking Catalyst Composition to Chirality Distributions of as-Grown Single-Walled Carbon Nanotubes by Tuning NixFe1-x nanoparticles. *Nat. Mater.* **2009**, *8*, 882−886.
(11) Ding, L.; Yuan, D.; Liu, J. Growth of High-Density Parallel Arrays of Long Single-Walled Carbon Nanotubes on Quartz Substrates. *J. Am. Chem. Soc.* **2008**, *130*, 5428−5429.
(12) Rutkowska, A.; Walker, D.; Gorfman, S.; Thomas, P. A.; Macpherson, J. V. Horizontal Alignment of Chemical Vapor-Deposited SWNTs on Single-Crystal Quartz Surfaces: Further Evidence for Epitaxial Alignment. *J. Phys. Chem. C* **2009**, *113*, 17087−17096.
(13) Yuan, D.; Ding, L.; Chu, H.; Feng, Y.; McNicholas, T. P.; Liu, J. Horizontally Aligned Single-Walled Carbon Nanotube on Quartz from a Large Variety of Metal Catalysts. *Nano Lett.* **2008**, *8*, 2576−2579.
(14) Burgos, J. C.; Balbuena, P. B. Preferential Adsorption of Zigzag Single-Walled Carbon Nanotubes on the ST-Cut Surface of Quartz. *J. Phys. Chem. C* **2013**, *117*, 4639−4646.
(15) Li, P.; Zhang, J. Sorting out Semiconducting Single-Walled Carbon Nanotube Arrays by Preferential Destruction of Metallic Tubes using Water. *J. Mater. Chem.* **2011**, *21*, 11815−11821.
(16) Xiao, L.; Schneider, W. F. Surface Termination Effects on Metal Atom Adsorption on α-Alumina. *Surf. Sci.* **2008**, *602*, 3445−3453.
(17) Hirunsit, P.; Balbuena, P. B. Effects of Water and Electric Field on Atomic Oxygen Adsorption on Pt−Co Alloys. *Surf. Sci.* **2009**, *603*, 3239−3248.
(18) Kresse, G.; Furthmuller, J. Efficient Iterative Schemes for Ab Initio Total-Energy Calculations using a Plane-Wave Basis Set. *Phys. Rev. B* **1996**, *54*, 11169−11186.
(19) Kresse, G.; Furthmuller, J. Efficiency of Ab-Initio Total Energy Calculations for Metals and Semiconductors using a Plane-Wave Basis Set. *Comput. Mater. Sci.* **1996**, *6*, 15−50.
(20) Blochl, P. E. Projector Augmented-Wave Method. *Phys. Rev. B* **1994**, *50*, 17953−17979.
(21) Perdew, J. P.; Burke, K.; Ernzerhof, M. Generalized Gradient Approximation Made Simple. *Phys. Rev. Lett.* **1996**, *77*, 3865−3868.
(22) Blochl, P. E.; Jepsen, O.; Andersen, O. K. Improved Tetrahedron Method for Brillouin-zone Integrations. *Phys. Rev. B* **1994**, *49*, 16223−16233.
(23) Materials Studio. 4.3 ed.; Accelrys Software Inc., 2008.
(24) Hamada, N.; Sawada, S.-i.; Oshiyama, A. New One-Dimensional Conductors: Graphitic Microtubules. *Phys. Rev. Lett.* **1992**, *68*, 1579.
(25) Saito, R.; Fujita, M.; Dresselhaus, G.; Dresselhaus, M. S. Electronic Structure of Chiral Graphene Tubules. *Appl. Phys. Lett.* **1992**, *60*, 2204−2206.
(26) Blase, X.; Benedict, L. X.; Shirley, E. L.; Louie, S. G. Hybridization Effects and Metallicity in Small Radius Carbon Nanotubes. *Phys. Rev. Lett.* **1994**, *72*, 1878.
(27) Phatak, A. A.; Delgass, W. N.; Ribeiro, F. H.; Schneider, W. F. Density Functional Theory Comparison of Water Dissociation Steps on Cu, Au, Ni, Pd, and Pt. *J. Phys. Chem. C* **2009**, *113*, 7269−7276.
(28) Andersson, K.; Ketteler, G.; Bluhm, H.; Yamamoto, S.; Ogasawara, H.; Pettersson, L. G. M.; Salmeron, M.; Nilsson, A. Autocatalytic Water Dissociation on Cu(110) at Near Ambient Conditions. *J. Am. Chem. Soc.* **2008**, *130*, 2793−2797.
(29) Mahadevan, T. S.; Garofalini, S. H. Dissociative Chemisorption of Water onto Silica Surfaces and Formation of Hydronium Ions. *J. Phys. Chem. C* **2008**, *112*, 1507−1515.
(30) Kim, Y. D.; Wei, T.; Stultz, J.; Goodman, D. W. Dissociation of Water on a Flat, Ordered Silica Surface. *Langmuir* **2003**, *19*, 1140−1142.
(31) Wang, G.-C.; Tao, S.-X.; Bu, X.-H. A Systematic Theoretical Study of Water Dissociation on Clean and Oxygen-Preadsorbed Transition Metals. *J. Catal.* **2006**, *244*, 10−16.
(32) Andersson, K.; Nikitin, A.; Pettersson, L. G. M.; Nilsson, A.; Ogasawara, H. Water Dissociation on Ru(001): An Activated Process. *Phys. Rev. Lett.* **2004**, *93*, 196101.
(33) Michaelides, A.; Alavi, A.; King, D. A. Different Surface Chemistries of Water on Ru{0001} From Monomer Adsorption to Partially Dissociated Bilayers. *J. Am. Chem. Soc.* **2003**, *125*, 2746−2755.
(34) Du, M. H.; Kolchin, A.; Cheng, H. P. Water-silica surface interactions: A Combined Quantum-Classical Molecular Dynamic Study of Energetics and Reaction Pathways. *J. Chem. Phys.* **2003**, *119*, 6418−6422.
(35) Pauling, L. The Nature of Silicon-Oxygen Bonds. *Am. Mineral.* **1980**, *65*, 321−323.